2020 IEEE/RSJ International Conference on Intelligent Robots and Systems (IROS)
October 25-29, 2020, Las Vegas, NV, USA (Virtual)

An Energy-based Approach for the Integration of Collaborative Redundant Robots in Restricted Work Environments

Sebastian Hjorth † *, Johannes Lachner ‡§, Stefano Stramigioli ‡, Ole Madsen † and Dimitrios Chrysostomou †
†Department of Materials and Production
Aalborg University, Aalborg, Denmark
* Corresponding author E-mail: sshj@mp.aau.dk
‡Faculty of Electrical Engineering, Mathematics and Computer Science
University of Twente, Enschede, Netherlands
§Kuka Deutschland GmbH, Zugspitzstraße 140, 86165 Augsburg, Deutschland

***Abstract*—To this day, most robots are installed behind safety fences, separated from the human. New use-case scenarios demand for collaborative robots, e.g. to assist the human with physically challenging tasks. These robots are mainly installed in work-environments with limited space, e.g. existing production lines. This brings certain challenges for the control of such robots. The presented work addresses a few of these challenges, namely: stable and safe behaviour in contact scenarios; avoidance of restricted workspace areas; prevention of joint limits in automatic mode and manual guidance. The control approach in this paper extents an Energy-aware Impedance controller by repulsive potential fields in order to comply with Cartesian and joint constraints. The presented controller was verified for a KUKA LBR iiwa 7 R800 in simulation as well as on the real robot.**

***Index Terms*—Workspace restriction, Redundant manipulators, Collaborative robots, Impedance Control, Artificial potential fields, Energy-aware robotics.**

I. Introduction

In recent years the number of collaborative robots has increased and will continue to rise in multiple work environments, especially in industrial and medical settings [1], [2]. These collaborative robots (e.g. KUKA LBR iiwa, ABB YuMi and FANUC CRX) are no longer restricted to only operate in a static and well-defined environment behind a fence, such as classic serial manipulators (e.g. KUKA KR6 and Fanuc M16iB) are. Hereby, these robots share their workspace with humans and support/share various complex tasks with them, such as: positioning an object in a more ergonomic position for the workforce [3], place or remove sub-components on the product while an operator works on a different part on the same product [4].

As the mentioned examples show, the implementation possibilities of collaborative robots are plentiful. However, all these possibilities bring up a number of challenges [5]. Two of them are:

- Safe physical Human Robot interaction (pHRI): the operator can share one workspace with the robot and if necessary interfere with its operation
- Integration in areas with limited space, e.g. in existing production lines

These challenges result in constraints for the robotic system, given by the workspace and the manipulator itself. In areas with limited space, pHRI is unavoidable and even wanted, Therefore, it should be possible for the human co-worker to distort the execution of the robot task. Moreover, there are Cartesian constraints in the workspace where the robot should be kept out of. As in those areas clamping situations in case of an unintended collision could occur. Robot given constraints are e.g. singularities, self collisions and joint limits. If any of these constraints are violated, the manipulator stops its movement and must be reinitialized. In an efficient pHRI scenario, interacting without stability problems, due to singularities and joint limit violations, have to be ensured. Moreover, appropriate joint limit avoidance strategies reduce the risk of robot self collisions.

Different control strategies have been developed over the years to meet these challenges. These control strategies are implemented on different control levels, e.g. position, velocity, force and torque level. However, most of them focus only on some of these challenges.

The work [6]–[8] focus on the avoidance of pHRIs, by either adapting the manipulator's trajectory or Nullspace, while relying on external sensors (e.g. cameras and depth sensors). In [9], a closed-loop-inverse-kinematic control approach on velocity level is implemented that respects the manipulator's joint limits as well as Cartesian obstacles. The method proposed in [10] saturates the manipulator's Nullspace. It combines the stack of task approach with quadratic programming in order to keep the manipulator within a set of hard-constraints for the joint positions, velocities, and accelerations. This approach can also be used to restricting the manipulator's workspace. The approaches proposed in [11], [12] focus on an admittance control strategy to limit the manipulator's workspaces for planned/guided interactions only. Because of their non compliant behaviour in planned or unplanned contact, the controller in [6]–[12] show drawbacks for their use in pHRI.

For redundant manipulators, [13] proposes six-dimensional Cartesian workspace constrains using an invariance control

scheme in combination with a discrete-time Euler solver to reduce oscillations at the Cartesian constraint, as the discrete-time implementations of the invariance control suffers from so called chattering. In [14], a combination of impedance control, control-barrier-functions and quadratic programming was successfully used to enforce Cartesian workspace-restrictions for a redundant robot. Both approaches presented in [13] and [14] solely focus on the enforcement of Cartesian workspace constraints of the end-effector and do not include the constrains in the manipulator's joint space.

The work in [15] presents an Operational Space Control framework to handle joint limits and singularities. However, this framework does not include Cartesian constraints. One closely related work is [16]. It extends the Operational Space Control framework by hard constraints and transforming the algorithm in [10] to torque level.

None of the above presented approaches observe the energy in the robotic system or the energy exchange with its environment. However, this is a crucial aspect to ensure robot stability and safe pHRI.

The formalism presented in this paper will focus on an energy-based control strategy in order to tackle the aforementioned challenges. This will be done by combining the Energy-aware reactive control scheme presented in [17], [18] with the concept of artificial potential fields introduced in [19]. Compared to the related work this formalism has a clear advantage: it enables an autonomous adaption of the manipulator's compliant behaviour without external sensory input. The implemented Energy-aware control scheme observes, monitors and limits the energy introduced to the manipulator by the controller and its energy exchange with environment. This ensures a safe interaction since the energy exchange is limited to a specified threshold. As mentioned in [16], common problems of the potential field approach are occurring oscillations when a link moves along the activation zone of a constraint. In our work this drawback can be minimized by regulating the energy in the robot system. To summarize, the main contributions of the proposed work are:

- Cartesian workspace restriction and joint limit avoidance, valid for all links/joints
- Energy-based formulation of the control strategy ensures stable and safe robot behaviour
- Verification of the implemented control strategy on a redundant manipulator in simulation and the real world.

The remainder of the paper is structured as follows: Section II provides a general overview over the presented control strategy. In Section III the theory of the implemented control strategy is introduced. In Section IV the experimental results are shown while Section V concludes the findings of the experimental results.

Notation: Small bold letters and capital bold letters indicate vectors and matrices respectively. The transpose of $\mathbf{x}$ is represented as $\mathbf{x}^\top$. The wrench of frame c in respect to frame j expressed in i is indicated by $\mathbf{w}_c^{i,j}$. $\widehat{\mathbf{x}}$ is the skew-symmetric matrix representation of $\mathbf{x}$. $\mathbf{I}_f$ represents an identity matrix of dimension f.

II. Concept

Reactive control schemes merge the planning and execution phase of the robot [20]. Compared to traditional control schemes, these controllers provide a greater flexibility in terms of handling interactions with its environment, e.g. the human co-worker. An impedance controller is a reactive controller that can be described as a mass-spring-damper system with adjustable parameters [21]. Instead of controlling just a single state variable, an impedance controller creates a dynamic relationship between the different state variables, by controlling the impedance of the robotic system [22]. Therefore, it is possible to describe any interaction with such a system as an energy exchange between the manipulator and its environment.

The robot's equation of motion is given by

$$\mathbf{M}(\mathbf{q})\ddot{\mathbf{q}} + \bar{\mathbf{C}}(\mathbf{q},\dot{\mathbf{q}})\dot{\mathbf{q}} + \bar{\mathbf{G}}(\mathbf{q}) = \boldsymbol{\tau}^\top, \tag{1}$$

with $\mathbf{q} \in \mathbb{R}^n$ being the generalized joint positions and $\mathbf{M}(\mathbf{q}) \in \mathbb{R}^{n\times n}$ being the positive-definite mass matrix. $\bar{\mathbf{C}}(\mathbf{q},\dot{\mathbf{q}})\dot{\mathbf{q}} \in \mathbb{R}^n$ represents the centrifugal and Coriolis torques, $\bar{\mathbf{G}}(\mathbf{q}) \in \mathbb{R}^n$ the gravitational torques and $\boldsymbol{\tau}^\top \in \mathbb{R}^n$ the control torques, respectively. Hereby, n denotes the number of joints. The joint torques on the right hand side of (1) can be decompose to

$$\boldsymbol{\tau}^\top = \boldsymbol{\tau}_{\text{Control}}^\top - \boldsymbol{\tau}_{\text{CC}}^\top + \boldsymbol{\tau}_{\text{JLA}}^\top + \underbrace{\boldsymbol{\tau}_{\text{Coriolis}}^\top}_{\bar{\mathbf{C}}(\mathbf{q},\dot{\mathbf{q}})\dot{\mathbf{q}}} + \underbrace{\boldsymbol{\tau}_{\text{Gravity}}^\top}_{\bar{\mathbf{G}}(\mathbf{q})}, \tag{2}$$

with $\boldsymbol{\tau}_{\text{Control}}^\top$ being the control torques of the robot task, $\boldsymbol{\tau}_{\text{CC}}^\top$ incorporating the Cartesian workspace restrictions, $\boldsymbol{\tau}_{\text{JLA}}^\top$ representing the torques to avoid joint limits and $\boldsymbol{\tau}_{\text{Coriolis}}^\top$ and $\boldsymbol{\tau}_{\text{Gravity}}^\top$ being the compensation torques for Coriolis and Gravity.

An overview of the implemented control structure with all components of (2) can be seen in Fig. 1.

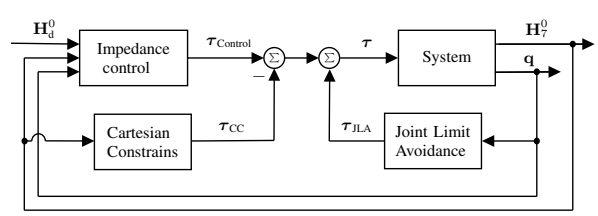

Fig. 1. The overall structure of the implemented control strategy.

III. Methods

The following section describes the mathematical derivation of the torque commands for the robot motion (III-A), including the Cartesian (III-B) and joint limit (III-C) constraints.

A. Control scheme

The presented controller includes methods such as Energy shaping and Damping injection [17]. These methods counteract autonomously the non-linear behavior of a normal Impedance controller, by observing the energy introduced to the manipulator and its power exchanged in contact with the environment [23], [24].

The resulting joint torques $\boldsymbol{\tau}_{\text{Control}}^{\top}$ of (2) can be decomposed to

$$\boldsymbol{\tau}_{\text{Control}}^{\top} = \boldsymbol{\tau}_{\text{Motion}}^{\top} - \boldsymbol{\tau}_{\text{Damping}}^{\top}, \tag{3}$$

where $\boldsymbol{\tau}_{\text{Motion}}^{\top} \in \mathbb{R}^n$ and $\boldsymbol{\tau}_{\text{Damping}}^{\top} \in \mathbb{R}^n$ are the torques generated by the motion generating springs and by the damping term, respectively.

1) Mathematical description of the motion generating springs: A wrench $\mathbf{w}_K^{7,7} \in se^*(3)$ generates the motion of the end-effector based on the end-effector's current transformation $\mathbf{H}_7^0 \in SE(3)$ and its desired goal transformation $\mathbf{H}_d^0 \in SE(3)$:

$$\mathbf{w}_K^{7,7\top} = \begin{bmatrix} \mathbf{f}_K^{7,7\top} \\ \mathbf{m}_K^{7,7\top} \end{bmatrix} = \begin{bmatrix} \mathbf{K}_t & \mathbf{K}_c \\ \mathbf{K}_c^{\top} & \mathbf{K}_r \end{bmatrix} \Delta\boldsymbol{\chi}, \tag{4}$$

with $\Delta\boldsymbol{\chi}^{\top} = \begin{bmatrix} \Delta\mathbf{o}_K^{7,7\top} & \Delta\boldsymbol{\theta}_K^{7,7\top} \end{bmatrix} \in se(3)$ being the infinitesimal body twist displacement, which can be extracted from $\left(\mathbf{H}_K^7\right)^{-1}\dot{\mathbf{H}}_K^7$ [23]. The elements $\mathbf{K}_t,\ \mathbf{K}_r \in \mathbb{R}^{3\times3}$ represent the stiffness for translation and rotation of the spring and $\mathbf{K}_c \in \mathbb{R}^{3\times3}$ is the decoupling between these two terms. In order to describe $\mathbf{w}_K^{7,7}$ purely in terms of energy, the force $\mathbf{f}_K^{7,7} \in \mathbb{R}^{1\times3}$ and momentum $\mathbf{m}_K^{7,7} \in \mathbb{R}^{1\times3}$ are formulated as

$$\begin{aligned}\widehat{\mathbf{f}}_K^{7,7} = &- \mathbf{R}_d^7 as\big(\mathbf{G}_t\widehat{\mathbf{p}}_7^d\big)\mathbf{R}_7^d - as\big(\mathbf{G}_t\mathbf{R}_d^7\widehat{\mathbf{p}}_7^d\mathbf{R}_7^d\big) \\ &- 2as\big(\mathbf{G}_c\mathbf{R}_7^d\big)\end{aligned} \tag{5}$$

and

$$\begin{aligned}\widehat{\mathbf{m}}_K^{7,7} = &- 2as\big(\mathbf{G}_r\mathbf{R}_7^d\big) - as\big(\mathbf{G}_t\mathbf{R}_d^7\widehat{\mathbf{p}}_7^d\widehat{\mathbf{p}}_7^d\mathbf{R}_7^d\big) \\ &- 2as\big(\mathbf{G}_c\widehat{\mathbf{p}}_7^d\mathbf{R}_7^d\big).\end{aligned} \tag{6}$$

Where $\mathbf{p}_7^d \in \mathbb{R}^3$ is the translation between the end-effector and its desired position and $\mathbf{G}_{r,t,c}$ are the co-stiffnesses for the translational spring, the rotational spring and the coupling terms, respectively. The operator $as()$ returns the anti-symmetric part of a square matrix. The co-stiffnesses are introduced for the convention between $\Delta\boldsymbol{\chi}$ and the Rotation matrices $\mathbf{R} \in SO(3)$:

$$\mathbf{G}_{r,t,c} = \frac{1}{2}tr\big(\mathbf{K}_{r,t,c}\big)\mathbf{I}_3 - \mathbf{K}_{r,t,c}. \tag{7}$$

The elastic wrench $\mathbf{w}_K^{7,7\top}$ can be mapped to the inertial reference frame by the adjoint coordinate transformation $Ad_{\mathbf{H}_0^7}^{\top} \in \mathbb{R}^{6\times6}$,

$$\mathbf{w}_K^{0,7\top} = Ad_{\mathbf{H}_0^7}^{\top}\mathbf{w}_K^{7,7\top}. \tag{8}$$

The joint torques $\boldsymbol{\tau}_{\text{Motion}}^{\top}$ are calculated with the transposed of the spatial geometric Jacobian $\mathbf{J}_7^{0,0}(\mathbf{q}) \in \mathbb{R}^{6\times n}$ (9).

$$\boldsymbol{\tau}_{\text{Motion}}^{\top} = \mathbf{J}_7^{0,0\top}(\mathbf{q})\mathbf{w}_K^{0,7\top} \tag{9}$$

2) Energy Scaling: In the concept of Energy-aware control, the energy of the system is scaled in order to assign a strict minimum in the desired configuration [25]. The energy-based safety metric demands a limit on the total energy of the system. The total energy stored in system is $E_{\text{total}} = T_{\text{total}} + U_{\text{total}}$, with $T_{\text{total}} \in \mathbb{R}$ being the kinetic energy and $U_{\text{total}} \in \mathbb{R}$ being the potential due to spatial springs [26]. Based on E_{total} and a chosen maximum energy E_{max} which the system is allowed to store, a scaling parameter $\lambda \in \mathbb{R}$ is computed:

$$\lambda = \begin{cases} 1 & \text{if } E_{\text{total}} \leqslant E_{\text{max}} \\ \frac{E_{\text{max}} - T_{\text{total}}}{U_{\text{total}}} & \text{otherwise.} \end{cases} \tag{10}$$

with

$$\begin{aligned}U_{\text{total}} = &-tr\big(\mathbf{G}_r\mathbf{R}_7^d\big) + \Big(-\frac{1}{4}tr\big(\widehat{\mathbf{p}}_7^d\mathbf{G}_t\widehat{\mathbf{p}}_7^d\big) \\ &-\frac{1}{4}tr\big(\widehat{\mathbf{p}}_7^d\mathbf{R}_7^d\mathbf{G}_r\mathbf{R}_d^7\widehat{\mathbf{p}}_7^d\big)\Big) + tr\big(\mathbf{G}_c\mathbf{R}_d^7\widehat{\mathbf{p}}_7^d\big)\end{aligned}. \tag{11}$$

As the potential energy stored in the spatial springs U_{total} are proportional to the Co-stiffness $\mathbf{G}_{r,t,c}$ [23], it is sufficient to scale $\mathbf{G}_{r,t,c}$:

$$\mathbf{G}_{r,t,c} \leftarrow \lambda\mathbf{G}_{r,t,c}. \tag{12}$$

Therefore, the motion generating wrench $\mathbf{w}_K^{0,7\top}$ applied at the robot end-effector is changed.

3) Damping injection: Next to the energy in the system, the power of the robot must be monitored and if necessary limited. Therefore, the *damping injection* method is used. Whenever the power resulting from the manipulator's motion

$$P_{\text{motion}} = \big(\mathbf{J}_7^{0,0}(\mathbf{q})^{\top}\mathbf{w}_K^{0,7\top} - \mathbf{B}_{\text{init}}\dot{\mathbf{q}}\big)^{\top}\dot{\mathbf{q}} \tag{13}$$

exceeds a maximal power threshold P_{max} the damping torque in (3) is increased:

$$\boldsymbol{\tau}_{\text{Damping}}^{\top} = \beta\mathbf{B}_{\text{init}}\dot{\mathbf{q}}; \quad \mathbf{B}_{\text{init}} \in \mathbb{R}^{n\times n}. \tag{14}$$

Hereby, the scaling factor $\beta \in \mathbb{R}$ is defined as:

$$\beta = \begin{cases} 1 & \text{if } P_{\text{motion}} \leqslant P_{\text{max}} \\ \frac{\left(\mathbf{J}_7^{0,0}(\mathbf{q})^{\top}\mathbf{w}_K^{0,7\top}\right)^{\top}\dot{\mathbf{q}} - P_{\text{max}}}{\dot{\mathbf{q}}^{\top}\mathbf{B}_{\text{init}}\dot{\mathbf{q}}} & \text{otherwise.} \end{cases} \tag{15}$$

Note that the initial damping $\mathbf{B}_{\text{init}}$ should be monitored with eq. (15), once the robot starts moving toward the desired transformation $\mathbf{H}_d^0$. In this case $P_{\text{motion}} > 0$. Once the human stops and handguides the robot the damping is kept at $\mathbf{B}_{\text{init}}$.

B. Cartesian constraints

In this work, a modified version of an artificial repulsive potential field is introduced in order to implement workspace constraints. As the work does not focus on the path planning itself, but rather on the restriction of the manipulator's Cartesian workspace, the focus will be limited to repulsive artificial potential fields for the remainder of the work.

To keep the respective links of the manipulator within the predefined Cartesian constraints C_j, a repelling wrench $\mathbf{w}_{C_j}^{i,i}$ is introduced:

$$\mathbf{w}_{C_j}^{i,i\top} = \begin{bmatrix} \mathbf{f}_{C_j}^{i,i\top} \\ \mathbf{m}_{C_j}^{i,i\top} \end{bmatrix}. \tag{16}$$

Its deveriation is based on the concepts presented in [27] and its component can be calulated by

$$\widehat{\mathbf{f}}^{i,i}_{C_j} = -as\big(\mathbf{Q}_{C_j,t_i}\mathbf{R}^i_{C_j}\widehat{\mathbf{p}}^{C_j}_i\mathbf{R}^{C_j}_i\big) - \mathbf{R}^i_{C_j}as\big(\mathbf{Q}_{C_j,t_i}\widehat{\mathbf{p}}^{C_j}_i\big)\mathbf{R}^{C_j}_i \tag{17}$$

and

$$\widehat{\mathbf{m}}^{i,i}_{C_j} = -as\big(\mathbf{Q}_{C_j,t_i}\mathbf{R}^i_{C_j}\widehat{\mathbf{p}}^{C_j}_i\widehat{\mathbf{p}}^{C_j}_i\mathbf{R}^{C_j}_i\big). \tag{18}$$

Note that since only the translational motion is of interest, it is only necessary to express (17) and (18) in dependency of the translational Co-stiffness $\mathbf{Q}_{C_j,\mathrm{t}_i}$. However, because of the non isotropic spring, the co-stiffness $\mathbf{Q}_{C_j,\mathrm{t}_i}$ also generates a repelling moment. Hereby, $\mathbf{Q}_{C_j,\mathrm{t}_i} = \frac{1}{2}tr(\mathbf{L}_{C_j,\mathrm{t}_i})\mathbf{I}_3 - \mathbf{L}_{C_j,\mathrm{t}_i}$, with $\mathbf{L}_{C_j,\mathrm{t}_i} \in \mathbb{R}^{3\times 3}$ being the spring stiffness of the wrench $\mathbf{w}^{i,i\,\top}_{C_j}$. This repelling force is directly dependent on a repulsive potential field, which is defined by the potential function

$$\sigma_{C_j,i} = \begin{cases} \frac{1}{\gamma}\left(\frac{1}{d_{i,C_j}(\mathbf{q})} - \frac{1}{x_j}\right)^{\gamma} & \text{if } d_{i,C_j}(\mathbf{q}) \leq x_j \\ 0 & \text{otherwise,} \end{cases} \tag{19}$$

where $\gamma > 0$ represents the generated potential. The shortest Euclidean distance between the points $\mathbf{p}^0_i \in \mathbb{R}^3$ and its projection onto the constraint $\mathbf{p}^0_{i,C_j} \in \mathbb{R}^3$ is given by $d_{i,C_j}(\mathbf{q}) \in \mathbb{R}$. The activation distance of the constraint is denoted $x_j \in \mathbb{R}$.

This function serves as a transition function between the free and restricted motion and is defined as a non-negative smooth surface for any given joint configuration $\mathbf{q}$. The resulting potential $\sigma_{C_j,i} \in \mathbb{R}$ increases towards infinity as the ith constraint link of the manipulator approach the constraint C_j. These Cartesian constraints also referred to as *virtual walls* can be described by any smooth manifold $C \cong \mathbb{R}^3$.

The potential $\sigma_{C_j,i}$ is then used to scale the translational co-stiffnesses $\mathbf{Q}_{C_j,\mathrm{t}_i}$ used for the computation of the repelling force $\mathbf{w}^{i,i}_{C_j}$ (16) described in (17) and (18) as seen in (20).

$$\mathbf{Q}_{C_j,\mathrm{t}_i} \leftarrow \sigma_{C_j,i}\mathbf{Q}_{C_j,\mathrm{t}_i} \tag{20}$$

In order to being able to express the repelling wrench $\mathbf{w}^{i,i\,\top}_{C_j}$ generated by constraint C_j acting on the ith link in the inertial reference 0-frame, it can be mapped with the help of the adjoint coordinate transformation $Ad^{\top}_{\mathbf{H}^i_0}$:

$$\mathbf{w}^{0,i\,\top}_{C_j} = Ad^{\top}_{\mathbf{H}^i_0}\mathbf{w}^{i,i\,\top}_{C_j}. \tag{21}$$

All link and constraint specific wrenches, expressed in the inertial reference frame, can be mapped to their equivalent joint torque representation by

$$\boldsymbol{\tau}^{\top}_{\mathrm{CC}} = \Big(\sum_{i=1}^{n}\big(\sum_{j=1}^{z}\mathbf{J}^{0,0\,\top}_i(\mathbf{q})\mathbf{w}^{0,i\,\top}_{C_j}\big)\Big), \tag{22}$$

where $\mathbf{J}^{0,0}_i(\mathbf{q})$ is the spatial geometric Jacobian for the ith link and z the number of constraints acting on the ith link.

Both, (9) and (22), describe the mapping of the desired Cartesian behaviour into the robot's joint space. At this point one advantage for the control of kinematically redundant robots can be seen. The controller enables stable transitions of the robot in and out of singularities, since no inversions of the Jacobian matrix occurs.

C. Joint limit avoidance

The concept of *joint limit avoidance* has strong similarities to the concept of Cartesian constraints: once a joint comes in a critical area, a repelling torque is generated that forces the joint to stay within the predefined limits. In the remainder of this section, the mathematical description of this control scheme will be based on a single joint; for an in-depth description of multiple joints see [19].

The difference between the current position of joint q_i and its lower/upper joint limits $\underline{q}_{i,\text{limit}}/\bar{q}_{i,\text{limit}}$ serve as input for a function, that generates a torque into the opposite direction of the active constraint:

$$\tau_{\mathrm{JLA}_i} = \begin{cases} \frac{\Omega}{\underline{q}_i^2}\left(\frac{1}{\underline{q}_i} - \frac{1}{\underline{q}_{i,J}}\right) & \text{if } \underline{q}_i \leq \underline{q}_{i,J} \\ -\frac{\Omega}{\bar{q}_i^2}\left(\frac{1}{\bar{q}_i} - \frac{1}{\bar{q}_{i,J}}\right) & \text{if } \bar{q}_i \leq \bar{q}_{i,J} \\ 0 & \text{otherwise.} \end{cases} \tag{23}$$

Note that the repelling torques $\boldsymbol{\tau}^{\top}_{\mathrm{JLA}} \in \mathbb{R}^n$ not only depended on the distance between q_i and its minimal/maximal bounds, but also on a distance $\underline{q}_{i,J}/\bar{q}_{i,J}$ at which the constraints turn active and the scaling factor $\Omega > 0$. The distances $\underline{q}_i$ and $\bar{q}_i$ can be calculated by

$$\begin{aligned} \underline{q}_i &= q_i - \underline{q}_{i,\text{limit}} \\ \bar{q}_i &= \bar{q}_{i,\text{limit}} - q_i\ . \end{aligned} \tag{24}$$

IV. Experimental Results

The performance of the presented control framework is evaluated both in simulation using MATLAB and on the real robot KUKA LBR iiwa 7 R800. The robot is controlled via an external PC and communicates with KUKA's Fast-Research-Interface (FRI) [28]. For the validation, two different test scenarios are presented: firstly, the behaviour at the Cartesian constraint is shown in simulation and on the real robot (IV-A); secondly, the joint-limit-avoidance in a compliant state was tested on the physical system (IV-B). Table I shows the parameters of the implemented reactive control scheme and the constraints of all experiments. The maximum contact energy threshold E_{max} in our experiments was chosen according to the ISO/TS 15066:2016 [29] specified range of $0.52 - 2.5$J and the maximal power threshold P_{max} was chosen based on previous positive results of [18].

A. Cartesian constraint Experiment

To verify the concept of Cartesian constraints, the experiment was split into two tests. In the first experiment the manipulators end-effector is forced to violate two constraints simultaneously. In the second experiment multiple links of the manipulator are simultaneously forced into a single constraint.

1) Multi Cartesian constraints: In this test, the manipulator moves along a predefined trajectory. The respective virtual walls C_1 and C_2 are positioned in in a way that, on its path, the robot will violate these constrains. The experimental set-up and the predefined trajectory can be seen in Fig. 2.

The activation distance $d_{7,C_{1/2}}$ of the constraints C_1 and C_2

TABLE I
CONTROL VARIABLES USED DURING THE DIFFERENT EXPERIMENTS.

Reactive control scheme		
Translational spring stiffness	$\mathbf{K}_t$	$2000 \cdot \mathbf{I}_3$
Rotational spring stiffness	$\mathbf{K}_r$	$100 \cdot \mathbf{I}_3$
Coupling spring stiffness	$\mathbf{K}_c$	$0 \cdot \mathbf{I}_3$
max. allowed Energy	E_{max}	2 J
max. allowed Power	P_{max}	0.5 W
inital Damping coeff.	$\mathbf{B}$	$5 \cdot \mathbf{I}_7$
Cartesian constraint Experiment		
Virtual wall 1	C_1	$\begin{bmatrix}0.5\\1\\0\end{bmatrix}, \begin{bmatrix}0.5\\1\\0.9\end{bmatrix}, \begin{bmatrix}0.5\\-1\\0\end{bmatrix}, \begin{bmatrix}0.5\\-1\\0.9\end{bmatrix}$ m
Virtual wall 2	C_2	$\begin{bmatrix}0.5\\1\\0.9\end{bmatrix}, \begin{bmatrix}0.5\\1\\0.9\end{bmatrix}, \begin{bmatrix}-1\\-1\\0.9\end{bmatrix}, \begin{bmatrix}-1\\1\\0.9\end{bmatrix}$ m
Virtual wall 3	C_3	$\begin{bmatrix}0.5\\1\\0.1\end{bmatrix}, \begin{bmatrix}0.5\\1\\0.1\end{bmatrix}, \begin{bmatrix}-1\\-1\\0.1\end{bmatrix}, \begin{bmatrix}-1\\1\\0.1\end{bmatrix}$ m
Translational spring stiffness	$\mathbf{L}_{C_j,\mathrm{t}_i}$	$10 \cdot \mathbf{I}_3$
activation distance	$d_{0,C_{1/2/3}}$	0.05m
exponential	γ	2
Joint Limit Avoidance Experiment		
upper activation limit	$\bar{q}_{i,J}$	0.2 rad
lower activation limit	$\underline{q}_{i,J}$	0.2 rad
scaling factor	Ω	0.025

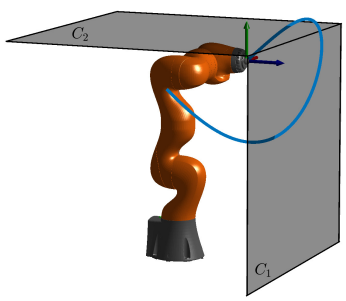

Fig. 2. The setup of the "Multi Cartesian constraint" test consists of a trajectory $\mathbf{H}_d^0(t)$ indicated as a blue line . As well as the constraints C_1/C_2 visualized as grey planes, which are placed respectively along the z-axis and x-axis in reference of the robots inertial reference frame.

was chosen to be 0.05m in order to have a sufficient buffer, such that the constraint is not being violated. The exponential of the transition function γ was set to 2, as it was stated in [19]. The initial spring stiffnesses of the repelling springs $\mathbf{L}_{C_{1/2},\mathrm{t}_7}$ are chosen to be 10 as early testing has shown that it is a sufficient value to keep the manipulator within the Cartesian constraints.

The resulting Cartesian motion of the manipulator's end-effector can be seen in Figs. 3a and 3b, for the simulation and real robot, respectively. It can be seen that the end-effector's movement deviates from the desired path when crossing the respective activation distance $d_{7,C_{1/2}}$ at time $t = 6$s/$t = 2$s. While the end-effector follows the trajectory along the constraint C_2, it encounters the constraint C_1 at time $t = 5.5$s for the simulation and $t = 5$s for the real-world test. At time $t = 8$s the robot no longer violates the virtual wall C_2 and the end-effector moves back on the z-component of the trajectory. However, in both scenarios the end-effector is only able to track the trajectory with an offset, until the trajectory no longer violates the constraint C_1 at $t = 15$s and $t = 14$s. This behaviour results from the implemented energy scaling method described in III-A2. Here, two benefits of the implemented control framework can be seen: the robot respects all Cartesian constraints while complying with the predefined energy and power for interaction. Moreover, thanks to energy scaling, no oscillations occur while moving along the constraints of C_1 and C_2, nor in the transition phase between C_1 and C_2, between 5-8s (cf. red zone in Fig. 3).

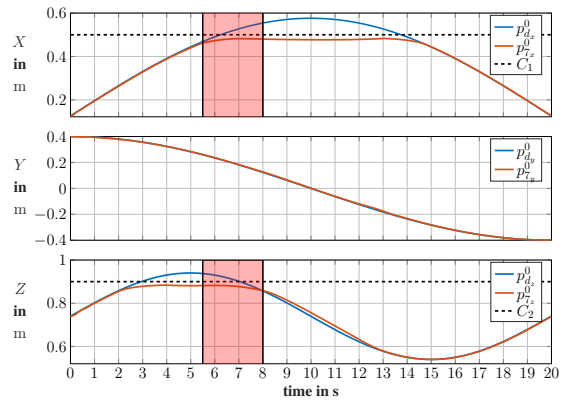

(a)

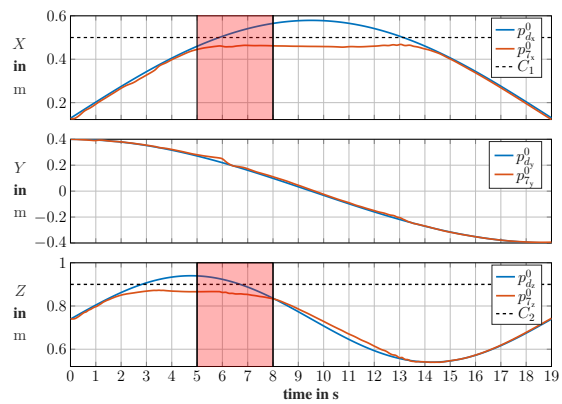

(b)

Fig. 3. The relationship of the trajectory and end-effector position for the simulation and real-world test are shown in (a) and (b), respectively. The virtual wall C_1 and C_2 only restricts the movements of the end-effector along the x-axis and z-axis of the base frame. The y-axis has no restriction.

With the energy E_{total} never exceeding the threshold E_{max} as seen in Fig. 4.

2) Multiple link restriction: This test validates the behaviour of manipulator when multiple links encounter a Cartesian constraints at the same point in time. The virtual walls C_3 is positioned in such a way that link 4, 6 and 7 can reach the constraint. Figure 5 shows how the manipulator is maneuvered until all three axes reaching the constraint.

In Fig. 6 it can be observed that even when multiple joints are pulled/pushed against the virtual wall for a period of 5.5s (cf. red zone in Fig. 6a), none of the respective links violate the constraint C_3. When all the respective links have crossed their respective activation distance d_{i,C_3} at around time $t = 11.5$s, the respective scaling factor $\sigma_{C_3,i}$ of the spring is increased and a repulsive force $\mathbf{w}_{C_3}^{0,i}$ is generated.

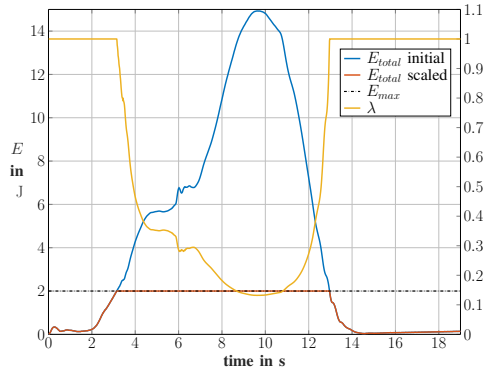

Fig. 4. The total energy E_{total} during the real-world Mutli-Cartesian constraint test. It can also be seen how λ limits E_{total} to E_{max}.

Fig. 5. The experimental setup for the "Multiple link restriction" test, where links 4, 6 and 7 forced towards the constraint C_3 visualized as a grey plane.

This shows another benefit of the implemented controller: when the energy threshold is violated through pulling/pushing on the robot structure, the stiffness of the spatial spring is decreased and the robot can be freely moved. Once the robot is released, it automatically approaches back on the desired trajectory while complying with the specified safe energy threshold.

B. Joint limit avoidance

This experiment validates the behavior of the implemented joint limit avoidance strategy when approaching one or multiple joint limits. By exceeding the maximal specified energy threshold, the manipulator was brought into compliant state and multiple joints where manually forced into the repecitve joint limit (joints 2, 4 and 6). None of these joints violated these limits, even though all axes where manually pushed into the limit simultaneously over a period of 7s (cf. red zone in Fig. 7). When a joint reaches its respective activation-area by crossing over the upper/lower activation limit $\underline{q}_{i,J}/\overline{q}_{i,J}$, a torque in opposing direction is generated. Figure 7 depicts that the torque τ_{JLA_i} increases as the distance to the constraint $\underline{q}_i/\overline{q}_i$ decreases and vise versa. This correlation can be seen when comparing the individual joint position q_i and the respective generated torques τ_{JLA_i}. None of these joints show an oscillatory behaviour (cf. red zone in Fig. 7). For redundant manipulators, benefits through the combination of

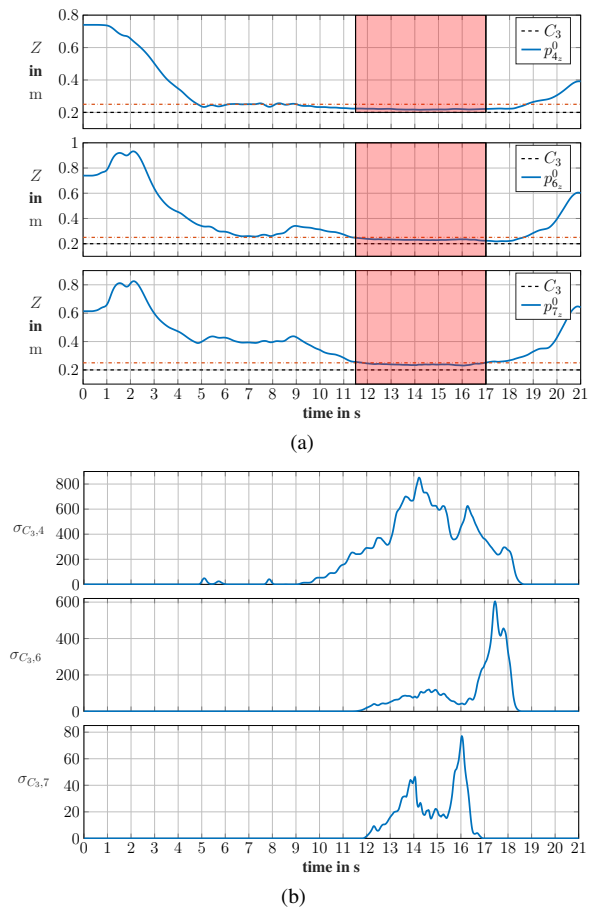

Fig. 6. The Cartesian position along the base frames z-axis for body 4, 6 and the 7 are shown in (a) and the respective repulsive field in (b).The virtual wall C_3 only restricts the movements of the links along the z-axis of the base frame. x-axis and y-axis are not restricted. The red dash dotted line in (a) indicates the distance at which the constraint activates or deactivates.

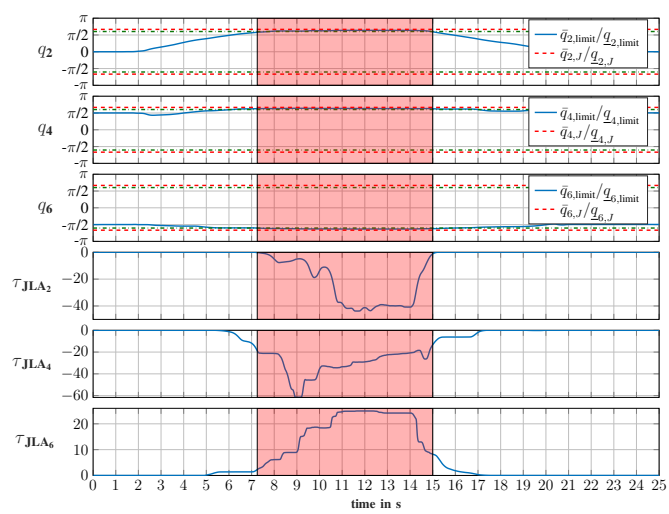

Fig. 7. The joint position of joints 2, 4, 6 and the torques generated by the implemented joint limit avoidance feature are visualized. The area marked in red indicates the time interval in which all joints encounter there respective limits simultaneously.

the energy-aware control scheme and the joint limit avoidance algorithm can be seen. When the energy threshold is violated

during a pHRI, the stiffness of the spatial spring is decreased and the nullspace of the manipulator autonomously adapts through the repelling torques of the joint limit avoidance algorithm.

V. Conclusions

This paper presents an energy-based control formalism for the integration of collaborative redundant robots in restricted work environments. It extends the concept of artificial potential fields by combining it with an Energy-aware reactive control scheme. The presented control framework is capable of handling planned and unplanned pHRI within a workspace with restricted areas. Therefore, no external sensors are needed.

The results of the experiments can be summarized as follows:

- In an unplanned collision, the presented controller reacts in a compliant manner, without exceeding predefined energy thresholds. After contact, the robot automatically re-positions on the trajectory.
- During pHRI, the robot can manually be guided by the human. The presented controller keeps the robot from violating its joint limits. This also holds, when multiple joints encounter their limits. No oscillatory behaviour could be monitored, when approaching the activation zone of the potential field.
- Restricted work environments yield Cartesian constraints for the robot. The controller was tested in scenarios with multiple restricted areas, where multiple links encountered Cartesian constraints. No oscillatory behaviour could be monitored, when approaching the activation zone of the potential field, nor in the transition phase between multiple constraints.

One drawback of the presented controller is that all relevant constraint parameters have to be tuned manually. If the manipulator is forced far from its desired configuration, the stiffness of the spatial spring are scaled close to 0. If the manipulator encounters joint limit constraint on its way back, the desired pose will not be reached without manual guidance. However, in true pHRI scenarios the human co-worker can assist in such cases.

In future work a safe recovery motion planner for handling such events could investigate. Furthermore, an extensive comparison between this work and other approaches, e.g. nullspace saturation algorithms could be done. Also the presented controller could be extended to incorporate more complex shaped Cartesian constraints. Lastly, the effects of the scaling functions in eq. (10) and eq. (15) and the effect of the repulsive forces on the passivity of the system have to be investigated, as for a passive robot, the energy and power thresholds can also be adapted online.

References

[1] A. M. Zanchettin, E. Croft, H. Ding, and M. Li, "Collaborative Robots in the Workplace," *IEEE Robotics and Automation Magazine*, vol. 25, no. 2, pp. 16–17, 2018.

[2] A. Ajoudani, A. M. Zanchettin, S. Ivaldi, A. Albu-Schäffer, K. Kosuge, and O. Khatib, "Progress and prospects of the human–robot collaboration," *Autonomous Robots*, vol. 42, no. 5, pp. 957–975, 2018.

[3] W. Kim, J. Lee, L. Peternel, N. Tsagarakis, and A. Ajoudani, "Anticipatory Robot Assistance for the Prevention of Human Static Joint Overloading in Human-Robot Collaboration," *IEEE RA-L*, vol. 3, no. 1, pp. 68–75, 2018.

[4] C. Schou, R. S. Andersen, D. Chrysostomou, S. Bøgh, and O. Madsen, "Skill-based instruction of collaborative robots in industrial settings," *Robotics and Computer-Integrated Manufacturing*, vol. 53, pp. 72–80, 2018.

[5] A. De Santis, B. Siciliano, A. De Luca, and A. Bicchi, "An atlas of physical human-robot interaction," *Mechanism and Machine Theory*, vol. 43, no. 3, pp. 253–270, 2008.

[6] J. H. Chen and K. T. Song, "Collision-Free Motion Planning for Human-Robot Collaborative Safety under Cartesian Constraint," *IEEE ICRA*, pp. 4348–4354, 2018.

[7] C. T. Landi, F. Ferraguti, S. Costi, M. Bonfe, and C. Secchi, "Safety barrier functions for human-robot interaction with industrial manipulators," *ECC 2019*, pp. 2565–2570, 2019.

[8] F. Chen, P. Di, J. Huang, H. Sasaki, and T. Fukuda, "Evolutionary artificial potential field method based manipulator path planning for safe robotic assembly," *IEEE MHS*, pp. 92–97, 2009.

[9] C. Scheurer, M. D. Fiore, S. Sharma, and C. Natale, "Industrial implementation of a multi-task redundancy resolution at velocity level for highly redundant mobile manipulators," *IEEE ISR*, vol. 2016, pp. 109–117, 2016.

[10] F. Flacco, A. De Luca, and O. Khatib, "Control of Redundant Robots under Hard Joint Constraints: Saturation in the Null Space," *IEEE Trans. Robot.*, vol. 31, no. 3, pp. 637–654, 2015.

[11] P. Chotiprayanakul, D. K. Liu, D. Wang, and G. Dissanayake, "A 3-dimensional force field method for robot collision avoidance in complex environments," *ISARC*, pp. 139–145, 2007.

[12] K. P. Tee, R. Yan, and H. Li, "Adaptive admittance control of a robot manipulator under task space constraint," *IEEE ICRA*, no. 1, pp. 5181–5186, 2010.

[13] M. Kimmel, M. Lawitzky, and S. Hirche, "6D Workspace Constraints for Physical Human-Robot Interaction using Invariance Control with Chattering Reduction," *IEEE IROS*, pp. 3377–3383, 2012.

[14] M. Rauscher, M. Kimmel, and S. Hirche, "Constrained Robot Control Using Control Barrier Functions," *IEEE IROS*, pp. 279–285, 2016.

[15] H. Han and J. Park, "Robot control near singularity and joint limit using a continuous task transition algorithm," *Int. J. Adv. Robot. Syst.*, vol. 10, pp. 1–10, 2013.

[16] J. D. Muñoz Osorio, F. Allmendinger, M. D. Fiore, U. E. Zimmermann, and T. Ortmaier, "Physical Human-Robot Interaction under Joint and Cartesian Constraints," *ICRA*, pp. 185–191, 2019.

[17] S. Stramigioli, "From differential manifolds to interactive robot control," Ph.D. dissertation, University of Twente, 12 1998.

[18] G. Raiola, C. A. Cardenas, T. S. Tadele, T. De Vries, and S. Stramigioli, "Development of a Safety- and Energy-Aware Impedance Controller for Collaborative Robots," *IEEE RA-L*, vol. 3, no. 2, pp. 1237–1244, 2018.

[19] O. Khatib, "Real-time obstacle avoidance for manipulators and mobile robots," vol. 2, 1985, pp. 500–505.

[20] O. Khatib, L. Sentis, J. Park, and J. Warren, "Whole-body dynamic behavior and control of human-like robots." *Int. J. of Humanoid Robotics*, vol. 10, pp. 29–43, 03 2004.

[21] O. Khatib and B. Siciliano, *Handbook of Robotics*. Springer, 2008.

[22] N. Hogan, "Impedance control: An approach to manipulation. part i, ii, iii," vol. 107, 07 1984, pp. 304 – 313.

[23] S. Stramigioli, *Modeling and IPC Control of Interactive Mechanical Systems - A Coordinate-Free Approach*. Springer, 2001.

[24] C. Ott, *Cartesian Impedance Control of Redundant and Flexible-Joint Robots*. Springer, Berlin, Heidelberg, 2008.

[25] C. F. Cristian Secchi, Stefano Stramigioli, *Control of Interactive Robotic Interfaces*. Springer, 2007.

[26] T. Tadele, "Human-friendly robotic manipulators: safety and performance issues in controller design," Ph.D. dissertation, University of Twente, 11 2014.

[27] E. D. Fasse and C. M. Gosselin, "On the spatial impedance control of gough-stewart platforms," pp. 1749–1754 vol.2, May 1998.

[28] G. Schreiber, A. Stemmer, and R. Bischoff, "The fast research interface for the kuka lightweight robot," in *IEEE ICRA*, 2010, pp. 15–21.

[29] "ISO/TS 15066:2016 robots and robotic devices — collaborative robots," 2016. [Online]. Available: https://www.iso.org/standard/62996.html